We are IntechOpen, the world's leading publisher of Open Access books Built by scientists, for scientists

4,800
Open access books available

122,000
International authors and editors

135M
Downloads

Our authors are among the

154
Countries delivered to

TOP 1%
most cited scientists

12.2%
Contributors from top 500 universities

CLARIVATE ANALYTICS BOOK CITATION INDEX INDEXED

WEB OF SCIENCE™

Selection of our books indexed in the Book Citation Index in Web of Science™ Core Collection (BKCI)

Interested in publishing with us?
Contact book.department@intechopen.com

Numbers displayed above are based on latest data collected.
For more information visit www.intechopen.com

5

Carrier Transport and Recombination Dynamics in Disordered Organic Light Emitting Diodes

Shih-Wei Feng[1] and Hsiang-Chen Wang[2]
[1]*Department of Applied Physics, National University of Kaohsiung, Taiwan, R.O.C.*
[2]*Graduate Institute of Opto-Mechatronics, National Chung Cheng University, Chia-Yi, Taiwan, R.O.C.*

1. Introduction

Organic light emitting diode (OLED) displays are forecast to be the promising display technology. They are thin, flexible, energy conserving, and suitable for large screen displays. For the developments of high-performance devices, high efficiency and good color purity are necessary. The emission wavelengths can be modified by blending dopants into the polymers light emitting diodes or by the incorporation of fluorescent dyes into the emissive layers for small molecule devices. The incorporation of fluorescent dyes into host materials has the advantages of efficient color tuning, good device efficiency, and narrow emission spectrum width [1-4].

In OLEDs, carriers are localized in molecules and charge transport is a hopping process [2]. Carrier mobility is determined by charge transport between neighboring hopping sites. The mobility usually shows the Poole-Frenkel characteristic [5]. By controlling the distance between hopping sites, carrier mobility can be adjusted [6]. At thermodynamic equilibrium, charge carriers mostly occupy the deep tail states of the density-of-states (DOS) distribution [7]. Carrier hopping occurs mostly via shallower states [8,9]. This shows that carrier density could affect mobility. Furthermore, dopants in OLEDs act as shallow trapping centers, which trap carriers and change the carrier density. Carrier trapping is the main emission mechanism in doped organic systems [10]. This also shows the dependence of the mobility on the dopant concentration. Although the efficiency of doped OLEDs has been improved, the carrier dynamics have not been well discussed [1-4]. To further improve the efficiency and lifetimes of OLEDs, the carrier transport as well as recombination dynamics of doped OLEDs should be well explored.

In this study, the dependences of carrier transport behavior and luminescence mechanism on dopant concentration of OLEDs were studied. In the lightly-doped sample, higher carrier mobility and better device performance were observed. This shows that dopants create additional hopping sites and shorten the hopping distance. At a higher dopant concentration, dopants tend to aggregate and the aggregations degrade the device performance. In addition, the observed decay rates and luminescence efficiencies of the

doped samples can be used to calculate the radiative and nonradiative decay rates. The trend suggests that the lightly-doped sample can exhibit better luminescence efficiency at higher applied voltage while the highly-doped sample shows poorer luminescence efficiency even operated at lower applied voltage. The resulting recombination dynamics can be used to explain the device characteristics and performance of the doped samples.

2. Sample Structures and Experimental Procedures

The OLEDs are fabricated by vacuum deposition of the organic materials onto an indium-tin-oxide (ITO)-coated glass at a deposition rate of l-2Å s^{-1} at l0^{-6} Torr. The device structures are ITO/*N*, *N*'-bis(naphthalen-1-yl)-*N*, *N*'-bis(phenyl) benzidine (NPB：55nm) /Tris(8-quinolinolato)-aluminum(A1q_3) ： 10-(2-benzothiazolyl)-1, 1, 7, 7-tetramethyl-2, 3, 6, 7-tetrahydro-lH, 5H, 11H-benzo[*l*]pyrano[6, 7, 8-*i j*] quinolizin-11-one (C545T：40nm)/Alq_3 (40nm)/LiF(1nm)/Al(200nm). NPB and Alq_3 are used as the hole transport layer (HTL) and electron transporting layer (ETL), respectively. The dopant concentrations of C545T in A1q_3 are 1%, 3%, and 7%. The active areas of each device were 9 mm^2. A blank sample (no doping) was also prepared for comparison. Figure 1 shows the sample structures of OLEDs.

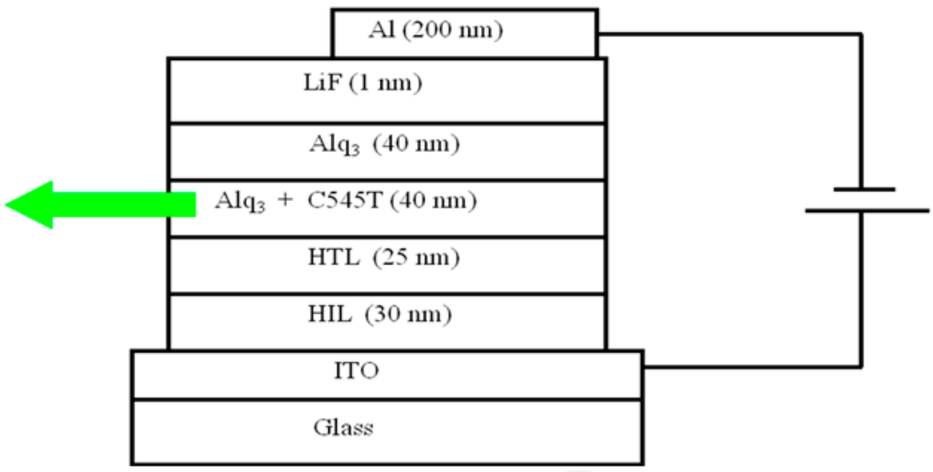

Fig. 1. Sample structures of OLEDs.

The morphological study was done by a scanning electron microscopy (SEM) (Hitachi Model S-4300N) with the excitation 5kV electrons. The electroluminescence (EL) spectra were measured by a Hitachi (model 4500) fluorescence spectrometer together with a power supply. Current-voltage (*I-V*) and capacitance-voltage (*C-V*) characteristics were measured with a semiconductor parameter analyzer (Agilent 4145B) and a LCR meter (Agilent 4284), respectively.

For transient electroluminescence measurements, a pulse generator (Agilent 8114A 100 V/2) was used to generate rectangular voltage pulses to the devices. The repetition rate and width of the pulse were l kHz and 5 μs, respectively. The light output was detected by a fast-biased silicon photodiode (Electro-Optics Technology Inc., model：ET-2020) operating directly on the surface of the devices. The transit time is a function of both the time required to charge the device (a function of the *RC* time constant of the circuit) and mobility [11]. In order to reduce the contribution of the time to charge the device, attention was paid to the

RC time constant of the EL cells. The maximum measured capacitance, *C*, of the EL cells was about 6 nF. The series resistance of our cells was estimated to be about 10 Ω. Therefore, the *RC* time constant was estimated to be less than 60 ns and the selected pulse width was greater than the charging time of the devices [4,12]. The temporal evolutions of EL signals were recorded by the average mode of a 50Ω input resistance of a digital oscilloscope (Agilent Model DSO 6052A, 500 MHz/4Gs/s). The oscilloscope was triggered by the pulse generator. The two coaxial cables for measuring transit EL and voltage pulse were equal in length, so that the time delay, except for the intrinsic delay, was negligible. All the measurements were carried out at room temperature (RT).

3. Experimental Results

3.1 SEM Images and EL Spectra (9 pt, bold)

Figure 2 (a) and (b) shows the SEM images of 1% and 3% C545T-doped Alq_3 films, respectively. The morphology of 1% C545T-doped Alq_3 film shows a homogeneous and flat image while that of 3% C545T-doped Alq_3 shows aggregations. This shows that dopants tend to aggregate as the dopant concentration becomes higher.

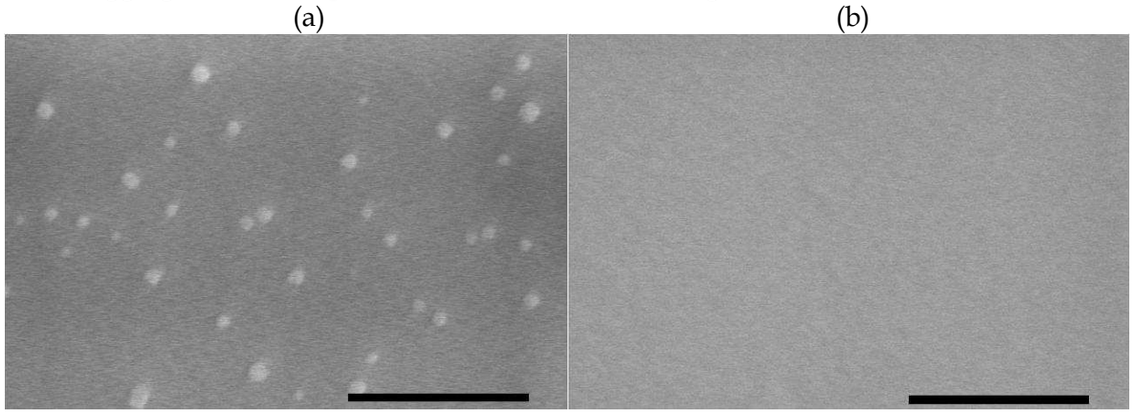

Fig. 2. SEM images of (a) 1% and (b) 3% C545T-doped Alq_3 films.

Figure 3 shows the EL spectra of 1%, 3%, and 7% C545T-doped Alq_3 samples and the undoped one. The EL spectra of the doped samples are significantly narrower than that of the undoped one. This is a tremendous advantage in the color mixing of red, green, and blue light for full-color applications. In order to create saturated colors, it is important for the individual red, green, and blue to be as pure as possible. Furthermore, as the dopant concentration increases, the peak position was slightly red-shifted and a shoulder in the long-wavelength side becomes apparent. Similar phenomena were also observed in Alq_3 films with 4-(dicyanomethylene)-2-methyl-6-(*p*-dimethylaminostyryl)-4H-pyran doapnt (DCM) aggregations [1,13,14]. The aggregations not only represent spatially distributed potential minimums but also broaden the effective DOS distribution. Hence, the broader spectrum width and the long-wavelength shoulder in EL spectra imply a larger degree of disorder.

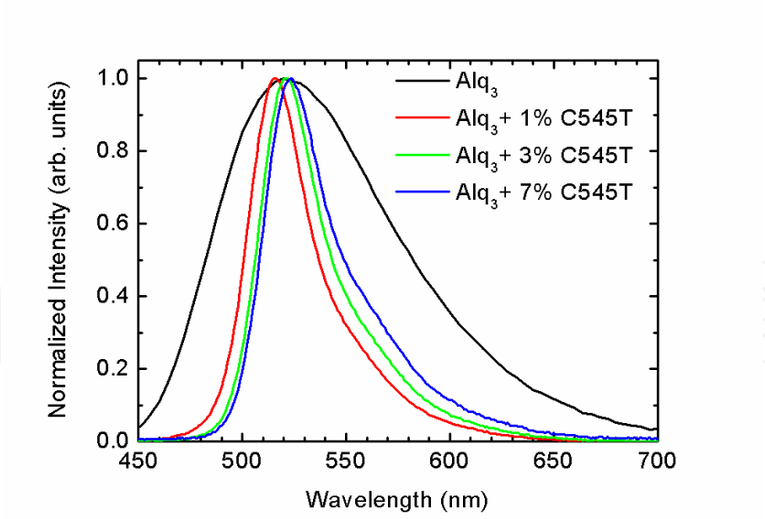

Fig. 3. EL spectra of the undoped and 1%, 3%, and 7% C545T-doped Alq_3 samples at RT.

3.2 *I-V* and *C-V* Characteristics

Figure 4(a) shows the current density versus applied voltage (*I-V*) characteristic of the four samples. Compared with the doped samples, the undoped sample shows a higher operational threshold and a shallow slope of current density versus applied voltage. This shows that the incorporation of dopants into host materials can improve device performance. In addition, with a higher dopant concentration, the driving voltage is higher and the current density is lower. This suggests that the aggregations tend to degrade the device performance.

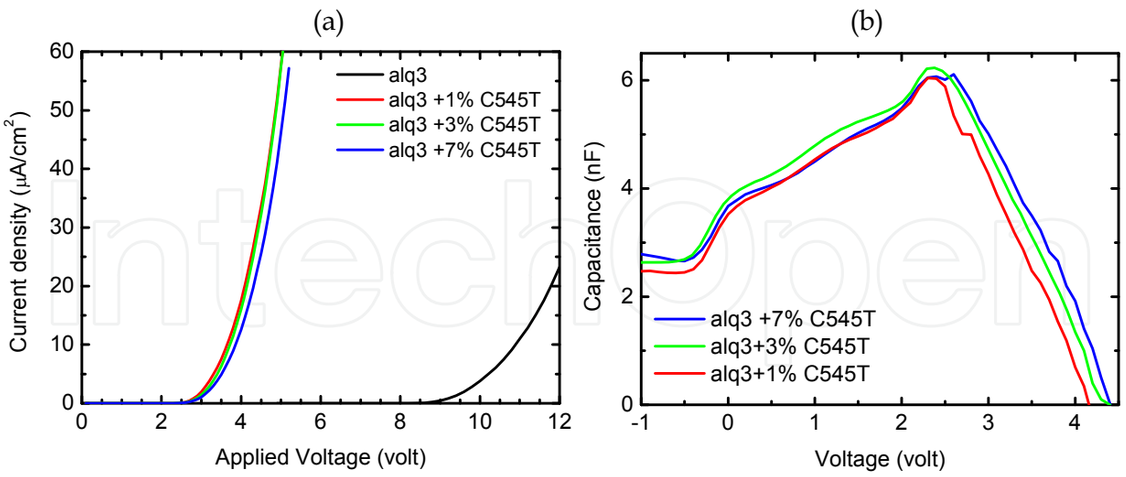

Fig. 4. (a) Current density versus applied voltage (*I-V*) characteristics of the undoped and three doped samples ; (b) the differential capacitance as a function of bias (*C-V*) at a fixed frequency of 10 Hz of the three doped samples.

Furthermore, Figure 4(b) shows the differential capacitance $C = dQ/dV$ as a function of bias for a fixed frequency 10 Hz. No apparent difference was observed for negative bias. For the positive bias, the capacitance increases significantly and reaches a maximum at the "transition voltage V_0". V_0 is regarded as the built-in voltage V_{bi}, ie. the difference in work function between the two contacts [15]. The transition voltages V_0 for 1%, 3% and 7% C545T-doped Alq_3 samples are 2.3, 2.38 and 2.6 volts, respectively. Aggregations can trap carriers for self-quenching and luminescence losses, which leads to a higher turn-on voltage in the highly-doped sample. This argument is consistent with the long-wavelength shoulder in the EL spectrum. Furthermore, as the applied voltage is beyond V_0, the electrons and holes start to recombine and the capacitance decreases. The negative slope is related to the recombination efficiency. The lower the capacitance, the better the recombination efficiency. The slower decreasing trend of the highly-doped samples implies a low recombination efficiency.

3.3 Carrier Transport and Recombination Dynamics

The dynamic behavior of EL under electrical fast-pulse excitation provides important insights into the carrier transport behaviors and internal operation mechanisms of OLEDs. The response time is determined by the time delay, t_d, between addressing the device with a short, rectangular voltage pulse and the first appearance of EL [16,17]. The EL onset is identified as the time at which the two leading fronts of injected holes and electrons meet in the device. The time after the EL tends to saturate is the time at which electron and hole distributions have interpenetrated. The temporal decay of the EL at the end of the applied voltage pulse reflects the depletion of the carrier reservoir established during the preceding on-phase. Because the doped samples performed better than the blank one, the discussions in this section were focused on the three doped samples.

Figure 5(a) shows the transient EL as a function of time for different applied voltages for 1% C545T-doped Alq_3 sample. With increasing applied voltage, a shorter time delay (i.e. an earlier EL onset) and a steeper rise of the transient EL were observed. This shows a faster response time and more carrier mobility.

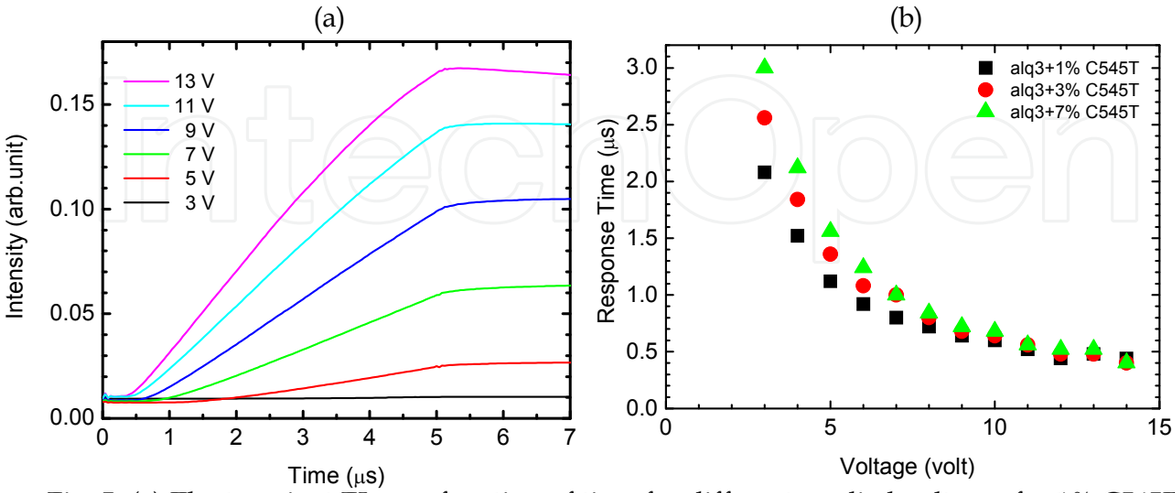

Fig. 5. (a) The transient EL as a function of time for different applied voltages for 1% C545T-doped Alq_3 sample. (b) Response time as a function of applied voltage for three doped samples.

The response time as a function of the applied voltage for the three samples are shown in Figure 5(b). At low applied voltages ($V_{applied} \le 8$ volts), the response time increases with dopant concentration. In the highly-doped sample, some carriers are trapped and then quenched in aggregations. This slows down carrier mobility and decreases the overlap integral of electron-hole wavefunctions. Hence, the response time is longer. On the other hand, with high applied voltages ($V_{applied} > 8$ volts), carriers have more mobility among the hopping sites so that carriers may not be quenched in aggregations. This leads to the response times nearly independent of dopant concentration. The constant response time within the large bias range ($V_{applied} \ge 11$ volts) implies a saturation of carrier mobility.

The transient EL decay as a function of time for different applied voltages for 1% C545T-doped Alq_3 sample is shown in Figure 6. The EL decay can be fitted with a single exponential to obtain decay time. Figure 7(a) shows the decay time as a function of applied voltage for the three doped samples. The decay rate ($\kappa = 1/\tau$), the reciprocal of the decay time (τ), is shown in Figure 7(b). The decay rate shows an increasing and then decreasing trend with increasing applied voltage. It is noted that the measured decay rate is the sum of the radiative decay rate and nonradiative decay rate by the following equation [18]：

$$\kappa = \kappa_r + \kappa_{nr} = \frac{1}{\tau} \tag{1}$$

where κ_r, κ_{nr}, and κ are the radiative decay rate, nonradiative decay rate, and total decay rate, respectively. At somewhat high applied voltages ($V_{applied} \ge 5$ volts), the slower decay rate may imply an enhanced nonradiative decay rate. The details will be discussed later.

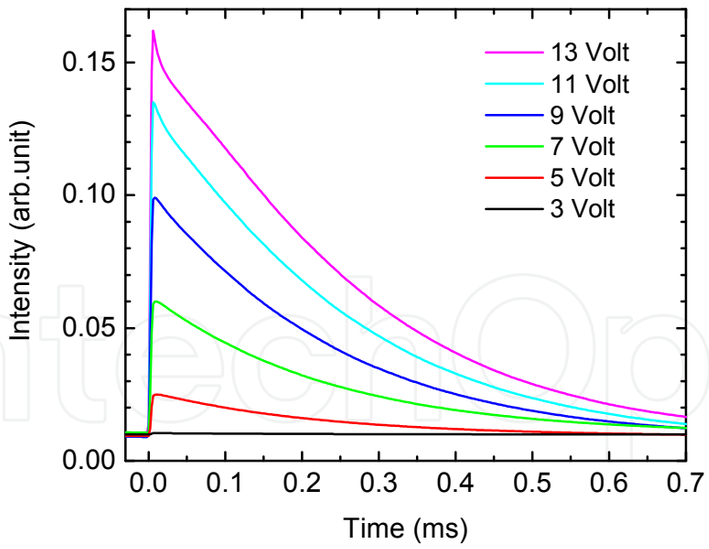

Fig. 6. The transient EL decay as a function of time for different applied voltages for 1% C545T-doped Alq_3 sample at RT.

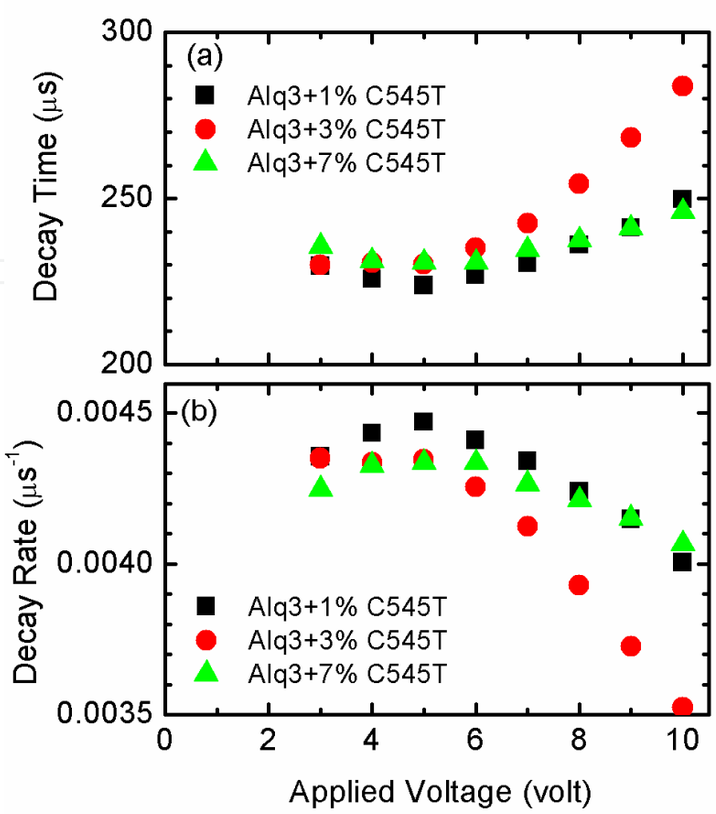

Fig. 7. (a) Decay times as well as (b) decay rates as a function of applied voltage for the three doped samples.

Figure 8 shows the luminescence efficiency as a function of applied voltage for the three doped samples. The luminescence efficiency exhibits a steep rise, then a substantial decrease with increasing current density. This phenomenon, called 'efficiency roll off' [19,20], was often observed in OLEDs and can be explained with the following mechanisms：(i) singlet-singlet and singlet-heat annihilations [21], (ii) exciton-exciton annihilation, (iii) excitons quenching by charge carriers, and (iv) field-assisted exciton-dissociation into an electron-hole pair [22]. In addition, the 1% C545T-doped Alq_3 sample has the best luminescence efficiency among the three samples. This shows that a small amount dopant improves the quantum efficiency. As the dopant concentration goes beyond a certain value, the dopants tend to aggregate. This degrades the device performance. Also, the response time seems to be related to the luminescence efficiency. Shorter response time correlates with luminescence efficiency. The shorter response time suggests higher carrier mobility and larger overlap integral of electron-hole wavefunctions. These factors improve the luminescence efficiency.

As shown in Figure 8, we normalize the luminescence efficiency at the maximum efficiency (at 3 volts) of 1% C545T-doped Alq_3 sample to get the normalized quantum efficiency. Because they have the same device structures, the extraction efficiencies of these samples are assumed to be the same and the normalized quantum efficiency can be regarded as the internal quantum efficiency. The internal quantum efficiency, η, is defined as the ratio of the number of light quanta emitted inside the device to the number of charge quanta

undergoing recombination. η is given by the radiative decay rate over the total decay rate of recombination [18,23]. The decay rate is the reciprocal of decay time $(\kappa = 1/\tau)$. Hence, η can be expressed as

$$\eta = \frac{\kappa_r}{\kappa_r + \kappa_{nr}} = \frac{\kappa_r}{\kappa} \tag{2}$$

where κ_r, κ_{nr}, and κ are the radiative decay rate, nonradiative decay rate, and total decay rate, respectively. η can be improved when the radiative decay rate, κ_r, is enhanced. Radiative recombination requires spatial overlap of the electron-hole wavefunctions and κ_r is expected to decrease when carrier separation occurs. κ_r is in the μs^{-1} to the ns^{-1} range when electron-hole pairs are located on a single conjugated polymer chain. It is difficult to give an order of magnitude to the nonradiative process, since it depends on the defect density. In order to quantitatively study the recombination dynamics, the observed decay rate (κ) and internal quantum efficiency (η) can be used to trace out the radiative decay rate and nonradiative decay rate by solving equations (1) and (2).

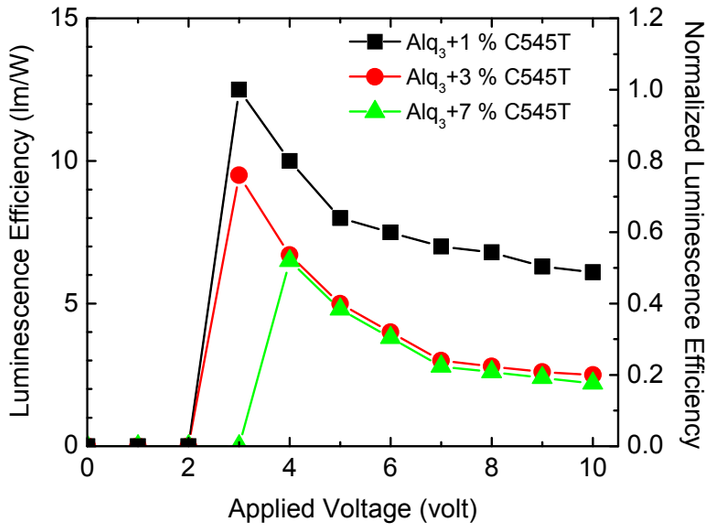

Fig. 8. Luminescence efficiency and normalized quantum efficiency as a function of applied voltage for the three doped samples.

Figure 9 shows the calculated results of κ_r and κ_{nr}. Some phenomena associated with recombination dynamics are shown in this figure. For the 1% C545T-doped Alq_3 sample, κ_r exhibits a decreasing trend with increasing the applied voltage while κ_{nr} does the opposite. Around the applied voltage $V_{1\%}$~7.5 volts, κ_r and κ_{nr} are equal, at about 0.0022 μs^{-1}. With the applied voltage lower than 7.5 volts, the larger κ_r implies better luminescence efficiency. At larger forward bias, the lower radiative decay rate and higher nonradiative decay rate are responsible for the lower luminescence efficiency of the OLED devices. The trends of κ_r and κ_{nr} can explain the luminescence efficiency as a function of applied voltage for the 1% C545T-doped Alq_3 sample, as shown in Figure 8. In addition, for the 3% and 7% C545T-doped Alq_3 samples, κ_r becomes lower while κ_{nr} is enhanced. At larger forward bias, the radiative decay rates, κ_r, are larger than nonradiative decay rates, κ_{nr}. These trends, due to the existence of aggregations, lead to the lower luminescence efficiency. For the 7% C545T-doped Alq_3 sample, the largest κ_{nr} and the smallest κ_r suggests the strongest nonradiative

recombination and poorest luminescence efficiency among the three doped samples. In addition, it was found that κ_r and κ_{nr} are equal, at about 0.0022 μs^{-1} for the three doped samples. The applied voltages $V_{3\%}$ and $V_{7\%}$, corresponding to equal κ_r and κ_{nr}, are ~4.3 and ~4.0 volts for the 3% and 7% C545T-doped Alq_3 samples, respectively. The applied voltages corresponding to equal κ_r and κ_{nr} decrease with increasing dopant concentration. These demonstrate that the lightly-doped sample exhibits better luminescence efficiency than the highly-doped samples at all applied voltages and that all the doped samples exhibit peak luminescence efficiency at relatively low applied voltage, with luminescence efficiency decreasing for all the doped samples as the applied voltage is increased. The resulting recombination dynamics are correlated with the device characteristics and performance of the doped samples.

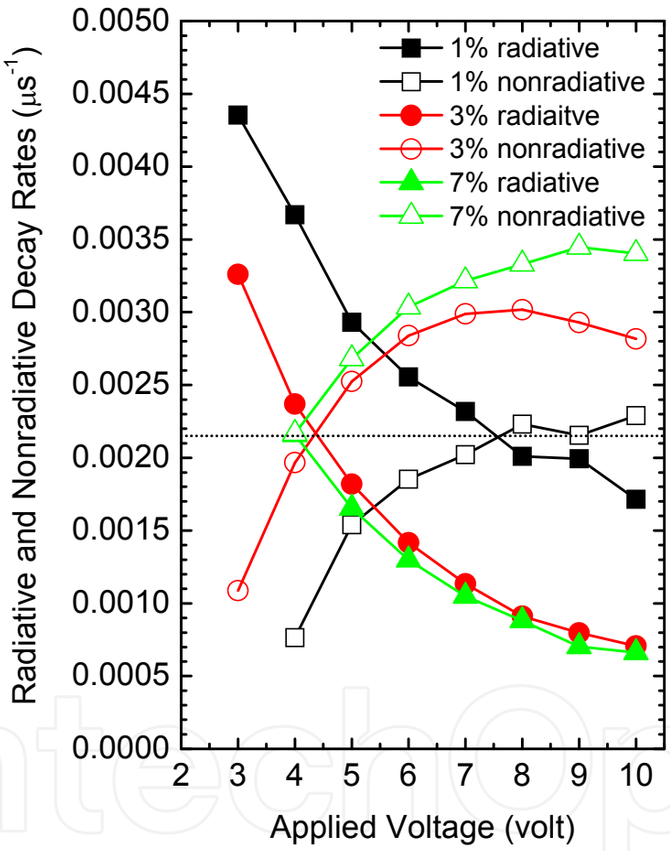

Fig. 9. Radiative decay rate (filled symbol) and nonradiative decay rate (empty symbol) as a function of applied voltage for the three doped samples.

4. Conclusion

In summary, the dependence of recombination dynamics and carrier transport on dopant concentration of OLEDs studied. In the lightly-doped sample, a higher carrier mobility and better device performance were observed. Due to the aggregations in the highly-doped samples, carrier quenching as well as nonradiative recombination degrade the device performance. In addition, the radiative decay rate and nonradiative decay rate were

calculated to explain the recombination dynamics. It was found that the lightly-doped sample exhibits better luminescence efficiency than the highly-doped samples at all applied voltages and that all the doped samples exhibit peak luminescence efficiency at relatively low applied voltage, with luminescence efficiency decreasing for all the doped samples as the applied voltage is increased. The results for recombination dynamics are correlated with the device characteristics and performance of the doped samples. The investigations are beneficial for discovering recombination dynamics, investigating quantum efficiency, and developing device applications.

5. References

1. A.A. Shoustikov, Y. You, and M.E. Thompson, IEEE Journal of Selected Topics in Quantum Electronics, 4 (1998) 3.
2. H. Bässler, Phys. Status Solidi B 175 (1993) 15.
3. J. Chen and D. Ma, J. Appl. Phys., 95 (2004) 5778.
4. D.G. Moon, R.B. Pode, C.J. Lee, and J.I. Han, Appl. Phys. Lett., 85 (2004) 4771.
5. A.B. Walker, A. Kambili, and S.J. Martin, J. Physics：Condens. Matter 14, (2002) 9825.
6. Y. Zhang, Y. Hu, J. Chen, Q. Zhou, and D. Ma, J. Phys. D 36 (2003) 2006.
7. V.I. Arkhipov, P. Heremons, E.V. Emelianova, G.J. Adriaenssens, and H. Bässler, Appl. Phys. Lett. 82 (2003) 3245.
8. D. Monroe, Phys. Rev. Lett. 54 (1985) 146.
9. V.I. Arkhipov, E.V. Emelianova, and G.J. Adriaenssens, Phys. Rev. B 64, (2003) 125.
10. M. Uchida, C. Adachi, T. Koyama, and Y. Taniguchi, J. Appl. Phys. 86 (1999) 1680.
11. C. Hosokawa, H. Tokailin, H. Higashi, and T. Kusumoto, Appl. Phys. Lett., 60 (1992) 1220.
12. R.A. Klenkler, G. Xu, H. Aziz, and Z.D. Popovic, Appl. Phys. Lett., 88 (2006) 242101.
13. K.H. Weinfurtner, H. Fujikawa, S. Tokito, and Y. Taga, Appl. Phys. Lett., 76 (2000) 2502.
14. E.M. Han, L.M. Do, M. Fujihira, H. Inada, and Y. Shirota, J. Appl. Phys., 80 (1996) 3297.
15. D.Y. Kondakov, J.R. Sandifer, C.W. Tang, and R.H. Young, J. Appl. Phys. 98 (2003) 1108.
16. W. Brütting, H. Riel, T. Beierlein, and W. Riess, J. Appl. Phys. 89 (2002) 1704.
17. M. Ichikawa, J. Amagai, Y. Horiba, T. Koyama, and Y. Taniguchi, J. Appl. Phys., 94, (2003) 7796.
18. E.F. Schubert, Light-Emitting Diodes, Cambridge University Press, 2006.
19. F.X. Zang, T.C. Sum, A.C. H. Huan, T.L. Li, W.L. Li, and F. Zhu, Appl. Phys. Lett., 93 (2008) 2339.
20. M. Cocchi, V. Fattori, D. Virgili, C. Sabatini, P. Di Marco, M. Maestri, and J. Kalinowski, Appl. Phys. Lett., 84 (2004) 1052.
21. H. Nakanotani, H. Sasabe, and C. Adachi, Appl. Phys. Lett., 86 (2005) 213506.
22. J. Szmytkowski, W. Stampor, J. Kalinowski, and Z.H. Kafafi, Appl. Phys. Lett., 80 (2002) 1465.
23. Q. Huang, S. Reineke, K. Walzer, M. Pfeiffer, and K. Leo, Appl. Phys. Lett., 89 (2006) 263512.

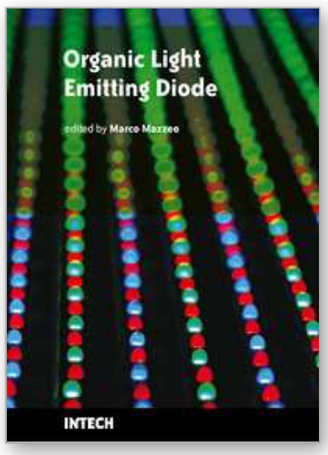

Organic Light Emitting Diode

Edited by Marco Mazzeo

ISBN 978-953-307-140-4
Hard cover, 224 pages
Publisher Sciyo
Published online 18, August, 2010
Published in print edition August, 2010

Organic light emitting diodes (OLEDs) have attracted enormous attention in the recent years because of their potential for flat panel displays and solid state lighting. This potential lies in the amazing flexibility offered by the synthesis of new organic compounds and by low-cost fabrication techniques, making these devices very promising for the market. The idea that flexible devices will replace standard objects such as television screens and lighting sources opens, indeed, a new scenario, where the research is very exciting and multidisciplinary. The aim of the present book is to give a comprehensive and up-to-date collection of contributions from leading experts in OLEDs. The subjects cover fields ranging from molecular and nanomaterials, used to increase the efficiency of the devices, to new technological perspectives in the realization of structures for high contrast organic displays and low-cost organic white light sources. The volume therefore presents a wide survey on the status and relevant trends in OLEDs research, thus being of interest to anyone active in this field. In addition, the present volume could also be used as a state-of-the-art introduction for young scientists.

INTECH
open science | open minds

InTech Europe
University Campus STeP Ri
Slavka Krautzeka 83/A
51000 Rijeka, Croatia
Phone: +385 (51) 770 447
Fax: +385 (51) 686 166
www.intechopen.com

InTech China
Unit 405, Office Block, Hotel Equatorial Shanghai
No.65, Yan An Road (West), Shanghai, 200040, China
中国上海市延安西路65号上海国际贵都大饭店办公楼405单元
Phone: +86-21-62489820
Fax: +86-21-62489821

IntechOpen